LA-UR-19-22533
Approved for public release; distribution is unlimited.

Title: Development of and initial assessment of microstructurally engineered UN

Author(s): Shivprasad, Aditya Prahlad
Grote, Christopher John
White, Joshua Taylor

Intended for: Report

Issued: 2019-07-23 (rev.2)

APPENDIX E

NTRD DOCUMENT COVER SHEET [1]

Name/Title of Deliverable/Milestone/Revision No.: M3FT-19LA020201024 Development and initial assessment of microstructurally engineered UN

Work Package Title and Number: FT-19LA02020102; Advanced Ceramic Fuel Development

Work Package WBS Number: 1.02.02.02.01; LWR Fuels

Responsible Work Package Manager: Joshua Taylor White (Digitally signed by Joshua Taylor White Date: 2019.03.21 15:23:35 -06'00') (Name/Signature)

Date Submitted 03/21/2019

Quality Rigor Level for Deliverable/Milestone[2]	☐ QRL-1 ☐ Nuclear Data	☐ QRL-2	☑ QRL-3	☐ QRL 4 Lab QA Program[3]

This deliverable was prepared in accordance with Los Alamos National Laboratory
(Participant/National Laboratory Name)

QA program which meets the requirements of
☑ DOE Order 414.1 ☐ NQA-1 ☐ Other

This Deliverable was subjected to:

☑ Technical Review ☐ Peer Review

Technical Review (TR)
Review Documentation Provided
☐ Signed TR Report or,
☐ Signed TR Concurrence Sheet or,
☑ Signature of TR Reviewer(s) below

Name and Signature of Reviewers
Scarlett Widgeon Paisner (Digitally signed by Scarlett Widgeon Paisner Date: 2019.03.21 15:25:14 -06'00')

Peer Review (PR)
Review Documentation Provided
☐ Signed PR Report or,
☐ Signed PR Concurrence Sheet or,
☐ Signature of PR Reviewer(s) below

Name and Signature of Reviewers

NOTE 1: *Appendix E should be filled out and submitted with each deliverable. Or, if the PICS: NE system permits, completely enter all applicable information in the PICS: NE Deliverable Form. The requirement is to ensure that all applicable information is entered either in the PICS: NE system or by using the NTRD Document Cover Sheet.*

- *In some cases there may be a milestone where an item is being fabricated, maintenance is being performed on a facility, or a document is being issued through a formal document control process where it specifically calls out a formal review of the document. In these cases, documentation (e.g., inspection report, maintenance request, work planning package documentation or the documented review of the issued document through the document control process) of the completion of the activity, along with the Document Cover Sheet, is sufficient to demonstrate achieving the milestone.*

NOTE 2: *If QRL 1, 2, or 3 is not assigned, then the QRL 4 box must be checked, and the work is understood to be performed using laboratory QA requirements. This includes any deliverable developed in conformance with the respective National Laboratory / Participant, DOE or NNSA-approved QA Program.*

NOTE 3: *If the lab has an NQA-1 program and the work to be conducted requires an NQA-1 program, then the QRL-1 box must be checked in the work Package and on the Appendix E cover sheet and the work must be performed in accordance with the Lab's NQA-1 program. The QRL-4 box should not be checked.*

Development of and initial assessment of microstructurally engineered UN

Nuclear Technology Research and Development

Prepared for
U.S. Department of Energy
FCRD Program
Aditya P. Shivprasad
Christopher J. Grote
Joshua T. White
Los Alamos National Laboratory

March 21, 2019
NTRD-M3FT-19LA020201024
LA-UR-19-22533

SUMMARY

Fuels with high uranium densities have been considered in the Nuclear Technology Research and Development program's Advanced Fuels Campaign as potential replacements for uranium(IV) oxide in commercial light water reactors. One such candidate fuel is uranium mononitride, UN, which has been observed to readily oxidize in steam and simulated pressurized water reactor conditions. Thus, it is important to examine methods for waterproofing UN, especially for potential cladding breach scenarios. This can be achieved by controlling the microstructure so as to prevent contact between the UN fuel and coolant.

Research so far this FY has focused on screening potential candidate additive materials to control UN microstructure using steam oxidation TGA. From these candidates, yttrium was selected based on corrosion resistance, which led to attempts to develop a method for liquid phase sintering of yttrium with UN. Yttrium in the form of yttrium dihydride (YH_2) was mixed with UN, pressed, and heated to temperatures above the melting point of Y metal to dehydride the material and then melt it to enable liquid phase sintering. Results showed no indication of densification, but did show chemical interaction between Y and UN, resulting in the formation of yttrium nitride (YN) and uranium metal. These observations were used to develop a better understanding of microstructure control for UN waterproofing to be addressed in an L2 milestone that is an FY19 deliverable (M2FT-19LA020201021).

CONTENTS

FIGURES

TABLES

ACRONYMS

PWR	Pressurized water reactor
FRL	Fuels Research Laboratory
XRD	X-ray diffraction
TGA	Thermogravimetric analysis/analyzer
PCT	Pressure-composition-temperature
PDF	Powder diffraction file
SEM	Scanning electron microscopy

DEVELOPMENT OF AND INITIAL ASSESSMENT OF MICROSTRUCTURALLY ENGINEERED UN

1. Introduction

Uranium mononitride, UN, is a promising candidate for accident tolerant fuels because of its high thermal conductivity and uranium density, as compared with uranium(IV) oxide (UO_2). Higher thermal conductivity results in lower fuel centerline temperatures during operation and, thus, lower stored energy of the reactor core. High uranium density results in an increased fission density and, thus, allows for a greater neutronic penalty from accident tolerant fuel claddings. Proposed accident tolerant claddings include stainless steel, Fe-Cr-Al (and derivative alloys), and silicon carbide because of their improved resistance to waterside corrosion compared to zirconium-based fuel cladding. However, all of these cladding concepts use elements with higher neutron absorption cross-sections than zirconium. Because of this, the improved fission density of uranium mononitride enables the use of these types of cladding in reactors. In addition to accident tolerance with respect to neutronics and thermal conductivity, it is important to assess the behavior of uranium mononitride in a cladding breach scenario. However, resistance of uranium mononitride to waterside corrosion during such conditions has been shown to be poor. In particular, uranium mononitride exposed to high-temperature steam and simulated pressurized water reactor (PWR) environments has been observed to degrade by rapid pulverization.

Previous work in FY18 within the campaign examined the performance of uranium mononitride in a variety of environments such as steam and high-temperature/pressure water with hydrogen water chemistry [1]. Steam tests were carried out *in-situ* using thermogravimetric analysis, while simulated PWR conditions were performed in-autoclave. Work within the campaign also examined the feasibility of waterproofing uranium mononitride by co-sintering with uranium(IV) oxide. Composites of UN/UO_2 were examined for waterside corrosion resistance, as well, showing decreased resistance with increasing uranium mononitride content, given the known resistance of UO_2 to waterside corrosion. Thermogravimetric analysis of UN/UO_2 composites in 62 - 83% steam (varies as a function of temperature for a specific water flowrate) under a temperature ramp to 1000 °C, as evaluated in FY17 work, is shown in Figure 1 for various uranium mononitride contents. Similar data for isotherms at 350 °C and 82% steam are shown in Figure 2. During isothermal waterside corrosion, mass gain and pulverization occurred over the course of minutes, though the addition of uranium(IV) oxide significantly delayed the onset of oxidation. Similarly, during temperature ramps in steam, the addition of UO_2 appeared to delay the onset of oxidation, though pulverization occurred for pellets containing more than 10 volume percent uranium mononitride. Based on these results, it is clear that additions of uranium(IV) oxide are not sufficient to waterproof uranium mononitride. These results drive the need for other methods of waterproofing uranium mononitride using a controlled microstructure.

Three concepts being developed to control the microstructure of uranium mononitride to prevent oxidation are: (1) sintering with a more electropositive metal (with a protective oxide) to act as a sacrificial anode during the corrosion reaction (i.e. cermet) , (2) sintering with a ceramic that is highly resistant to corrosion that will act to protect the fuel as a whole (co-sintering), and (3) coating pellets with a corrosion-resistant material, either metal or ceramic. Because of the much lower melting point of metals, as compared with UN, the first waterproofing method can facilitate liquid-phase sintering, while the second method is anticipated to be limited to co-sintering.

For this L3 milestone, the first waterproofing method was evaluated following screening studies of candidate additive materials. In particular, this study focused on liquid phase sintering yttrium metal with uranium mononitride, while X-ray diffraction (XRD) and scanning electron microscopy (SEM) were also used to determine the final phase composition and microstructure of the resultant pellets. To supplement the sintering study, steam oxidation tests were conducted on candidate waterproofing materials of well-defined geometry, as has been done in previous work at the Fuels Research Lab (FRL) at LANL [2], [3]. The purpose of these tests was to determine the corrosion resistance of these materials in the types of tests that would be performed at LANL on viable pellets of uranium mononitride composites.

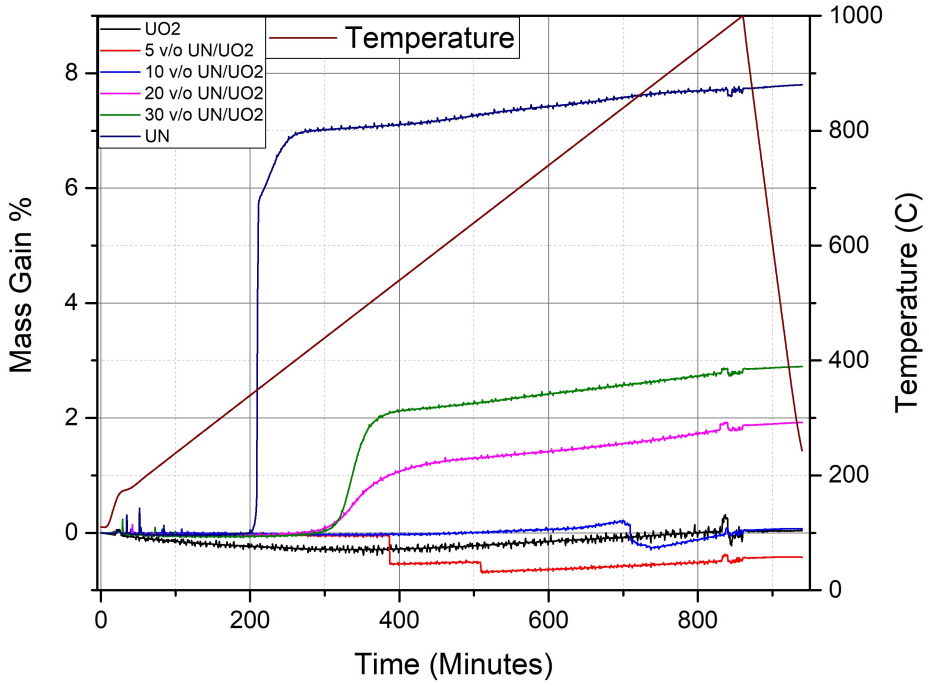

Figure 1: Thermograms comparing mass gain of composite materials (UN/UO_2) and monolithic UN and UO_2 during ramped heating to 1000 °C under 62 – 83% steam. Figure and caption adapted from [1].

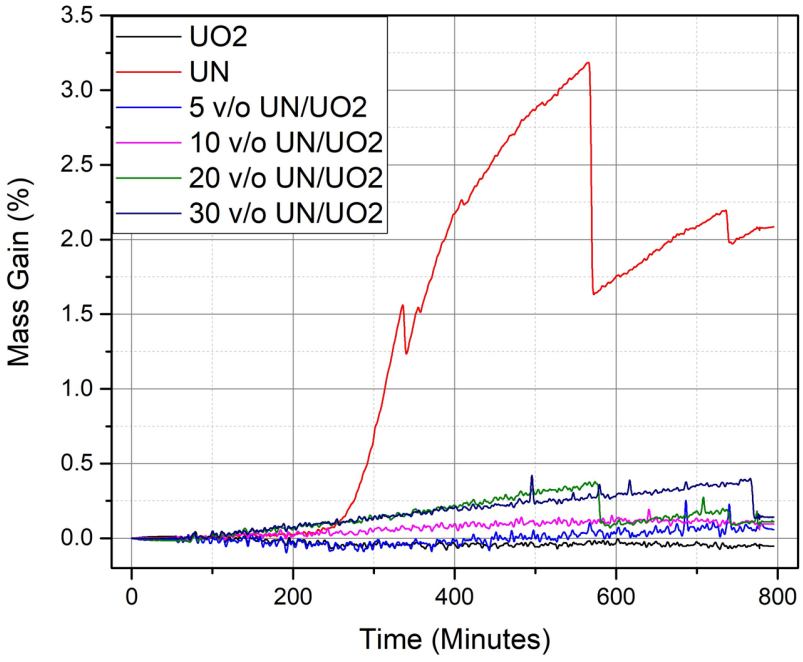

Figure 2: Isotherm data for monolithic UO_2, UN, and four composite materials collected at 350 °C under 82% steam for 12-hr. Figure and caption adapted from [1].

2. Experimental methods

2.1 Steam corrosion screening studies

Materials for steam corrosion testing were chosen based on oxidation resistance and the protective nature of the oxides. Candidate materials included yttrium metal, zirconium metal, silicon carbide, and APMT (Fe-Cr-Al variant) for the first round of experiments. Yttrium metal was obtained from GoodFellow USA (Coraopolis, PA, USA), while zirconium, silicon carbide, and APMT were legacy stock material available at LANL.

A simultaneous thermal analyzer (STA 449 F3, Netzsch Instruments, Selb, Germany) with a water vapor furnace and water vapor generator (DV2ML, Astream, Germany) was used to perform steam corrosion tests and measure mass change as a function of exposure time *in situ* at various temperatures. Pellets were placed in an alumina crucible to contain pulverized pellets during exposure and sample temperature was monitored using a type-S thermocouple. An image of the steam corrosion setup is shown in Figure 3.

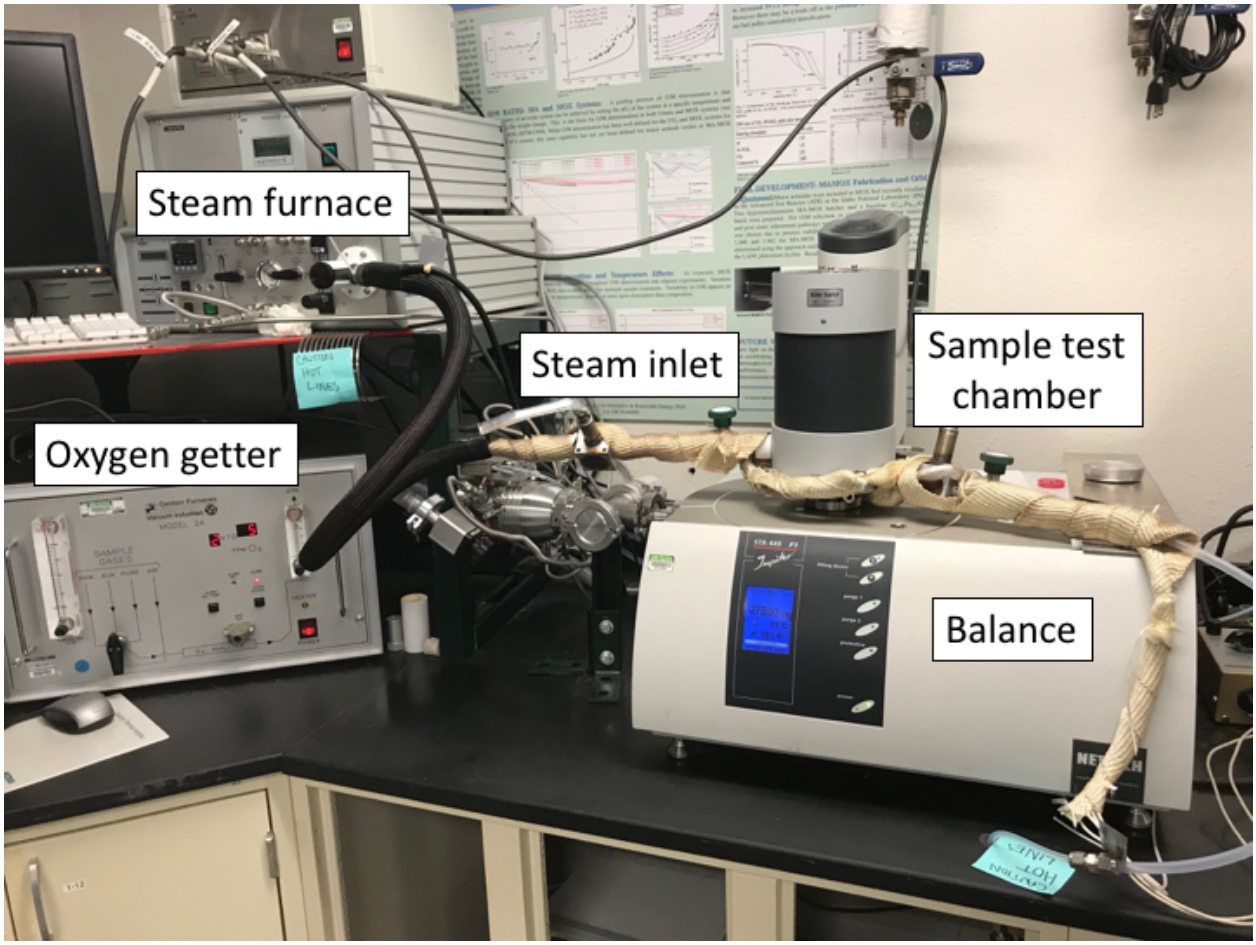

Figure 3: Experimental setup for steam TGA analysis. Annotations indicate major components of the system.

Samples were ramped up to 200 °C in gettered argon at 10 °C/min and allowed to stabilize for 30-min before introduction of steam. Temperature was increased from 200 °C to 1000 °C at 1 °C/min. Once the sample had achieved the maximum temperature, the steam was turned off and the sample was cooled in gettered argon to room temperature. For all tests, the water vapor flowrate was maintained at 9.14 g/hr of water. Gettered argon at 8 L/hr (calibrated with nitrogen) acted as a carrier gas for the steam, while a

protective gas of gettered argon at 20 mL/min was purged through the balance during each run. This resulted in a steam content ranging from 75% at 200 °C to 89% at 1000 °C.

2.2 Uranium mononitride-yttrium composite fabrication

Starting material used for this study was received from Areva (Courbevoie, France) as hyperstoichiometric uranium(IV) oxide, which was reduced to stoichiometric $UO_{2.00}$ under reducing conditions and converted to UN using the carbothermic reduction to nitridation process. Yttrium used in this study was high-purity legacy stock material (ca. 1960s) in the form of yttrium dihydride (YH_2) so as to aid in size-reduction processes. Trace element analysis of the yttrium stock was performed using inductively coupled plasma mass spectrometry (NSL Analytical Services, Cleveland, OH); results are summarized in Table 1. Yttrium dihydride purity was also confirmed using XRD (Figure 4) to have no detectable, unwanted phases (such as oxides or YH_3) within the resolution of the instrument.

Table 1: Trace element contents (in weight ppm) of Y metal used in this study. Contents are reported for tantalum, transition metals (TM) excluding Ta and Y, rare earth (RE) metals, and other elements (alkaline earth metals, alkali metals, other metals, non-metals, and metalloids, in order of concentration).

Element	Ta	TM (excl. Y, Ta)	RE metals	Other
Composition (wt. ppm)	2400	430	130	470

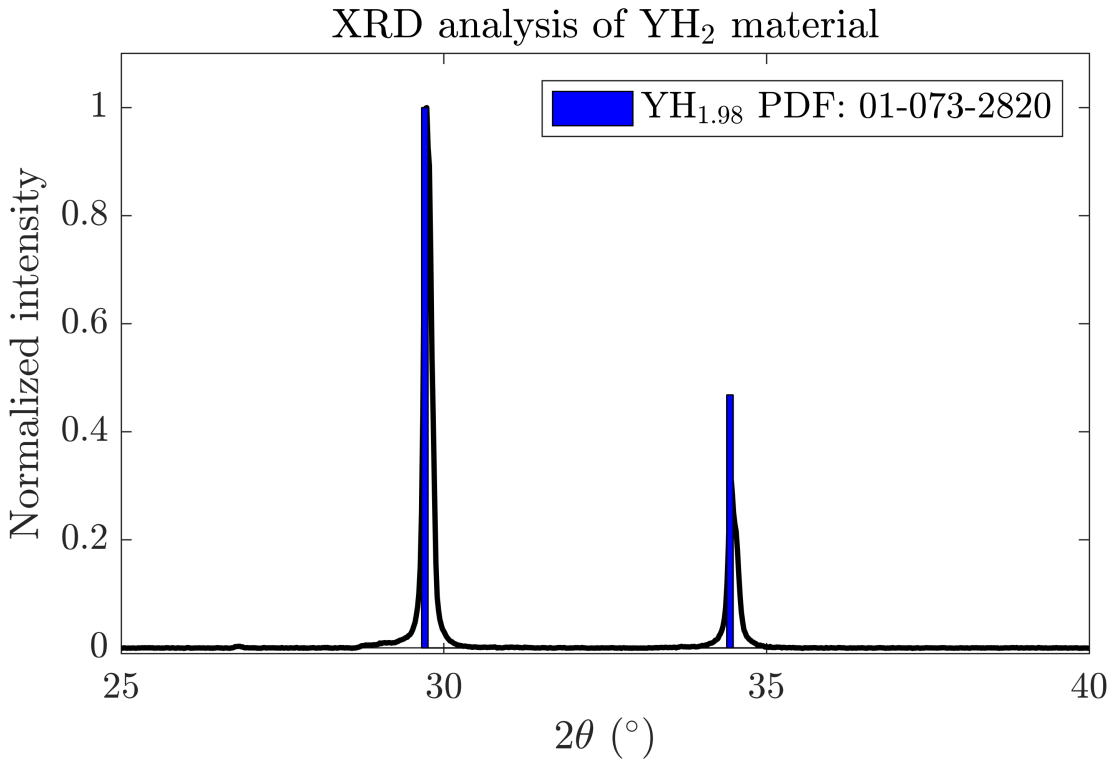

Figure 4: XRD pattern of as-received YH_2. No secondary phases were observed within the detection limit of the instrument.

Phase-pure uranium mononitride and yttrium dihydride were separately crushed in a silicon nitride and yttria-stabilized zirconia vial, respectively, using a high-energy ball mill (SPEX) for 30 minutes and subsequently sieved through a -325 mesh sieve (44-μm). The appropriate amounts of uranium mononitride and yttrium dihydride (see Table 2) were then co-milled for 5-minutes with 0.25 wt. %

ethylene bis(stearamide) (EBS) binder to mix the two materials. Theoretical densities were calculated using the rule of mixtures based on volume. Composite pellets were pressed at 150 MPa using a 5.2-mm punch and die set and then sintered above 1520 °C in gettered argon in a W-mesh furnace to facilitate melting of Y (T_m = 1526 °C). All material processing in this study was performed in an inert, argon glovebox. From previous work at the FRL, it was determined that yttrium dihydride, under inert conditions, will fully dehydride to yttrium metal by approximately 1000 °C with minimal volume change. This yttrium metal could then be used to liquid-phase sinter the uranium mononitride at or above the yttrium melting point.

Table 2: Calculated weight percent YH_2, composite theoretical densities, and experimental volume percent YH_2 for each batch of composite material.

Volume percent Y	Experimental mass YH_2 (g)	Experimental mass UN (g)	Experimental volume percent Y	Composite theoretical density (g/cm^3)
20 (1)	0.0950	1.2492	19.25	12.31
20 (2)	0.0878	1.0977	20.04	12.22
30	0.1327	0.9508	30.43	11.17
40	0.2310	1.1250	39.15	10.30

2.3 Microstructural analysis

XRD was used to analyze the phase content of the uranium mononitride-yttrium composites. A Bruker XRD (D2 Phaser, Bruker AXS, Madison, WI, USA) was used for these analyses. XRD scans were performed with 2θ ranging between 10 and 90° with a 0.01° 2θ-step and a 7-s acquisition time for each step. Material for all XRD examinations were homogenized using a mortar and pestle in an inert, argon glovebox and encapsulated in a low-background XRD sample holder to prevent exposure to air.

Scanning electron microscopy (SEM) was used to characterize the polished surface of one monolithic sample (UN-20Y) following attempted liquid phase sintering. A Phenom ProX SEM (Phenom World, Eindhoven, Netherlands) equipped with a backscatter detector and energy dispersive spectroscopy (EDS) was used for the microscopy analyses presented. The accelerating voltage during imaging was 15 kV to best image the secondary phases present. EDS was utilized to identify potential phase segregation and was also performed with an accelerating voltage of 15kV.

3. Results and discussion

3.1 Steam corrosion testing of candidate materials

Samples of cast Y metal, SiC, and APMT were exposed to steam using a temperature ramp to determine the protective nature of the oxide layer and the onset of breakaway oxidation. An archive test of zirconium sponge was compared to the results of this study to provide a baseline for oxidation performance in steam due to the use of zirconium-based alloys in-reactor and their well-characterized waterside corrosion performance. Results of the temperature ramp tests are given in Figure 5. This figure plots the extent of oxidation, which is defined as unity when all components of the material have oxidized, as a function of temperature. This requires an assumption on the type of oxide forming such that no hydroxides form and the oxides that form are not mixed oxides like spinel phases. For this analysis, it was assumed that zirconium oxidized to zirconium(IV) oxide, yttrium to yttrium(III) oxide, silicon carbide to silicon(IV) oxide and carbon dioxide, and Fe-Cr-Al oxidized to a weighted mixture of iron(III) oxide, chromium(III) oxide, and aluminum(III) oxide. Because of this, the y-axis in Figure 5 is reaction coordinate quantifying the extent of oxidation.

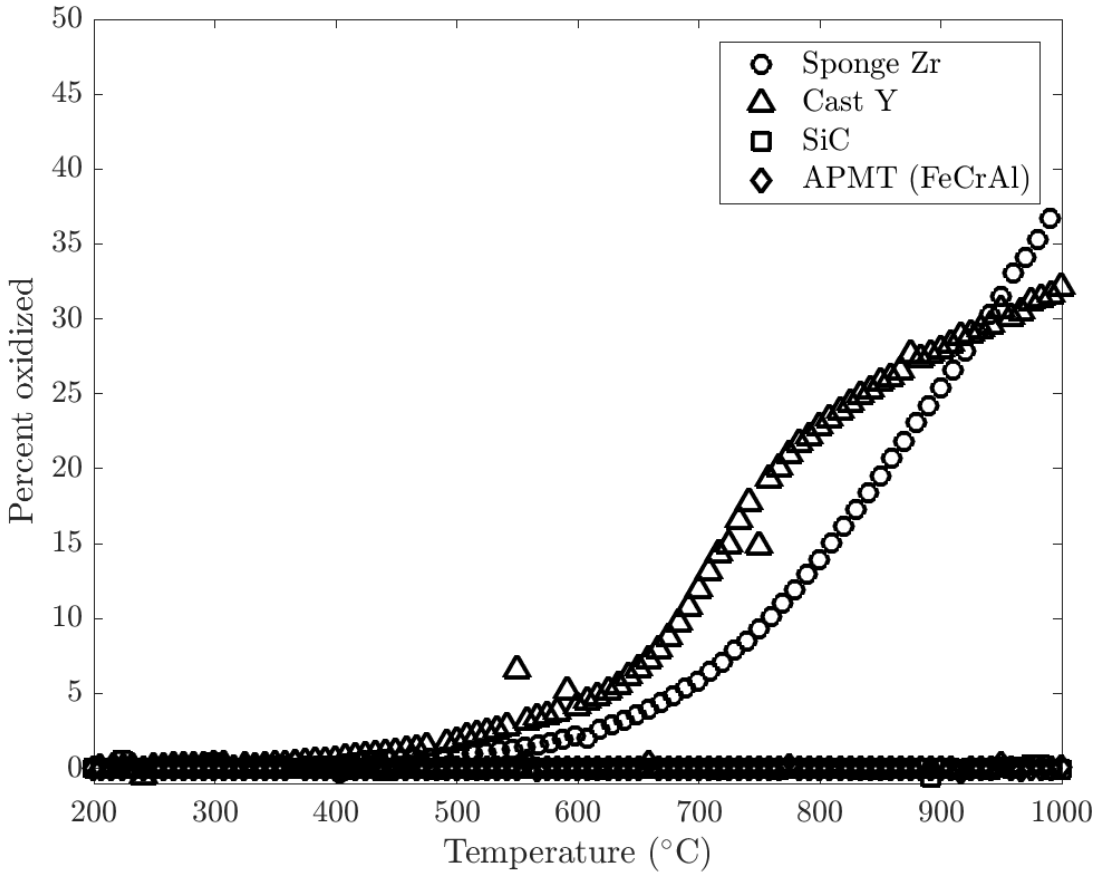

Figure 5: Thermograms comparing degree of oxidation (in percent oxidized) as a function of temperature for sponge Zr (archive), cast Y, SiC, and APMT during ramped heating to 1000 °C under 75% to 89% steam atmosphere.

Figure 5 shows that sponge zirconium and cast yttrium are the least resistant to oxidation under the test conditions considered here. Curiously, the yttrium begins to break away earlier than the zirconium, but exhibits smaller weight gains near 1000 °C than does the zirconium. One possibility is that yttrium

oxide is more protective at higher temperatures than is zirconium oxide. Another explanation is that the oxidation reaction product of yttrium is different between low- and high-temperature regimes, such as forming yttrium hydroxide at low temperature and yttrium(III) oxide at high temperature. Figure 6 shows before and after corrosion tested sample appearances. Before oxidation, the Y metal was polished to 10-μm grit to a mirror finish. After oxidation, the surface showed signs of a black oxide (substoichiometric yttria) with nodules of white oxide, likely indicating the initial formation of stoichiometric yttria. As expected, silicon carbide and APMT exhibited very strong resistance to corrosion.

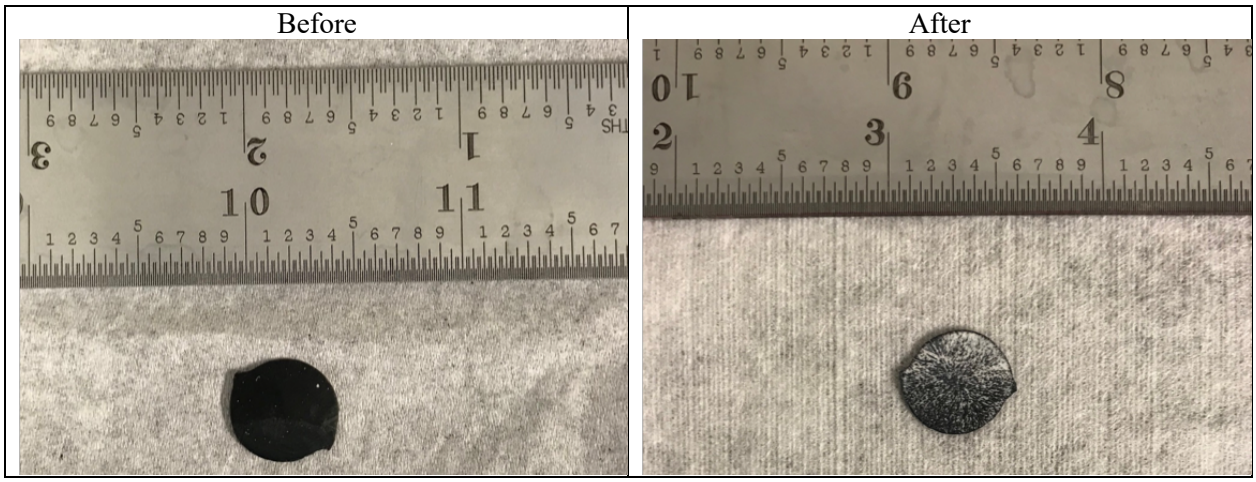

Figure 6: Appearance of Y metal after steam oxidation testing to 1000 °C in 75 - 89% steam.

From these results, APMT would be the best choice out of the tested metals for liquid phase sintering. However, APMT is difficult to mill, due to its ductility and, typically, Fe-Cr-Al alloys must be pre-aged in air to develop a protective oxide, which would have to be considered for composite design. This, compounded with the fact that yttrium and zirconium can form brittle hydrides that can be easily milled and can be dehydrided at elevated temperature to yield pure metal provided the basis for selecting either yttrium or zirconium for liquid phase sintering. The choice to pursue yttrium as the focus of this study to develop microstructurally-engineered uranium mononitride by liquid phase sintering was primarily driven by its improved high-temperature corrosion resistance, as compared to pure zirconium.

3.2 Uranium mononitride-yttrium composite phase content and microstructure

uranium mononitride-yttrium pellets were sintered at temperatures at or above the melting point of yttrium metal (1526 °C), which ranged from 1520 to 1540 °C. Final pellet densities were similar to those of the as-pressed state, but samples were slightly more robust. That is, as-pressed pellets would pulverize upon dropping, while ‘sintered’ pellets remained intact upon dropping. Table 3 summarizes the initial and final densities of pellet produced in this study. To answer why pellets were more robust despite no increase in density, samples were examined for phase content using XRD. A comparison between diffraction patterns for the three different compositions is shown in Figure 7.

Table 3: Comparison between the as-pressed and final densities for pellets produced for this study. Batch numbers correspond to those given in Table 2.

Pellet ID	Volume percent Y	As-pressed density (g/cm^3)	Anticipated percent TD (as-pressed)	Final density (g/cm^3)	Anticipated percent TD (final)
35-P-19-043	19.25	8.47	69.04	8.31	67.52
35-P-19-044	19.25	8.53	69.54	8.42	68.42
35-P-19-056	20.04	8.63	70.78	8.11	66.36
35-P-19-057	20.04	8.69	71.31	8.98	73.48
35-P-19-058	30.43	7.83	70.50	7.37	66.01
35-P-19-059	39.15	7.36	72.04	7.04	68.34
35-P-19-060	39.15	7.41	72.54	7.03	68.29

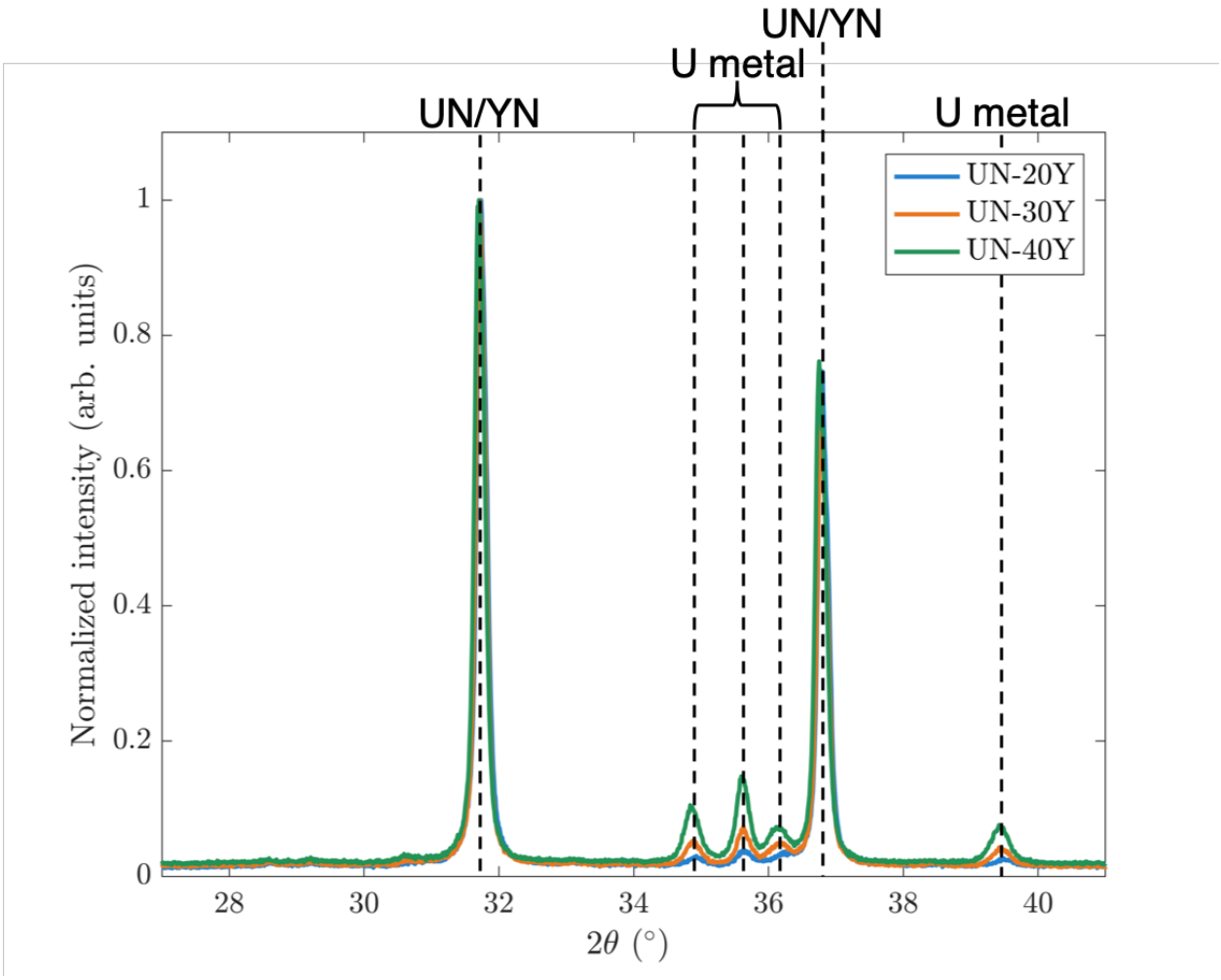

Figure 7: Comparison between XRD patterns for UN-20Y, UN-30Y, and UN-40Y. Evidence for the yttrium absorbing nitrogen from uranium mononitride is the increasing intensity of the uranium metal peaks.

The phases identified based on the diffraction patterns in Figure 7 were a combination of uranium nitride, yttrium nitride, and uranium metal. Yttrium nitride and uranium mononitride diffraction reflections are convoluted, which are the high-intensity peaks at 31.7 and 36.75° 2θ, while the low-intensity family of peaks from 35° - 36.2° and at 39.4° are associated with uranium metal.

There were no other peaks associated with yttrium-containing compounds. As such, it was determined that yttrium absorbed nitrogen from the uranium nitride to form yttrium nitride and uranium metal. Because the purpose of this study was to examine liquid phase sintering of yttrium, the result of yttrium nitriding was not expected. It is assumed that the reaction proceeded to completion, as no other yttrium-containing phases were observed.

To assess the regime where yttrium might absorb nitrogen from uranium, Gibbs free energy diagrams for the following reactions were calculated:

$$Y + UN \leftrightharpoons YN + U \quad (1)$$

$$YH_2 + UN \leftrightharpoons YN + U + H_2 \quad (2)$$

The thermodynamics of Equations (1) and (2) were assessed using ThermoCalc 2019a (Thermo-Calc Software AB, Solna, Sweden) and the SGTE Substances Database 6.0. Another reaction to consider is the denitriding of uranium mononitride to form a sub-stoichiometric mononitride where the offgassed nitrogen could react with yttrium metal. However, this type of reaction is difficult to implement in ThermoCalc without DFT modeling. Gibbs free energy was calculated for the two reactions. The results are shown below in Figure 8.

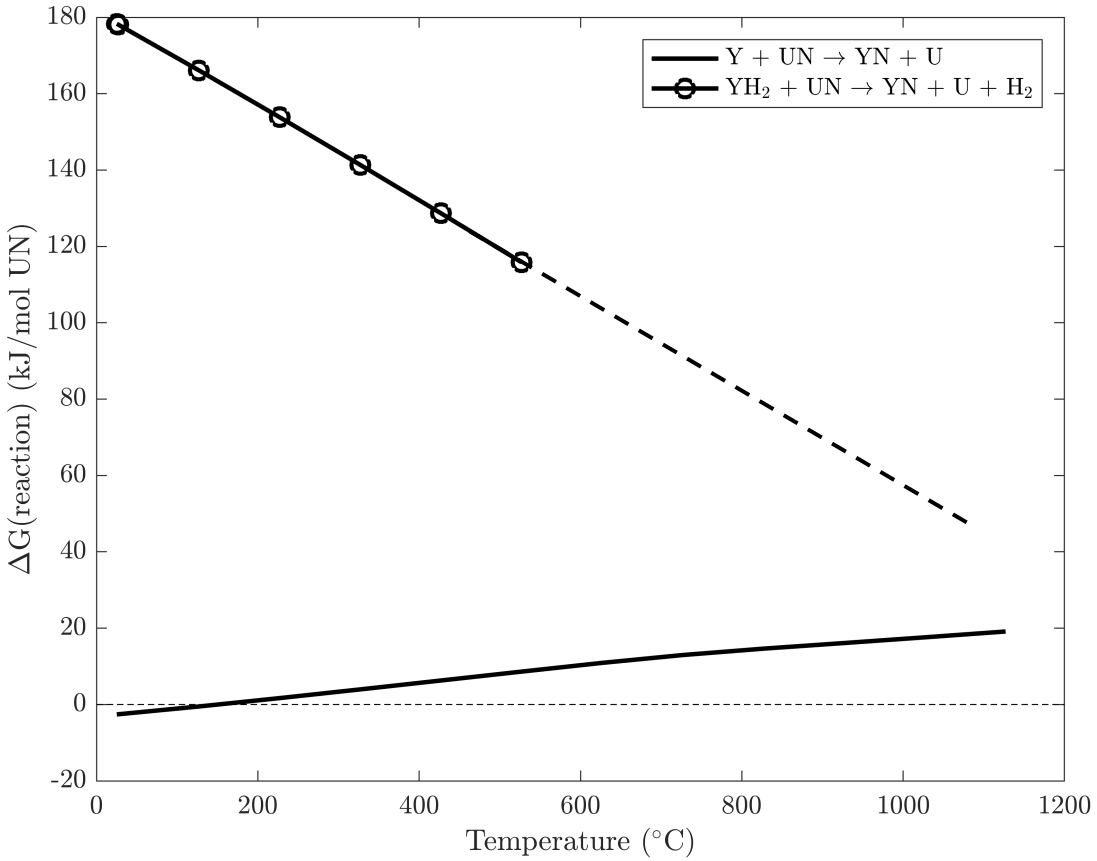

Figure 8: Gibbs free energy of reaction for nitriding reactions from yttrium metal and yttrium dihydride based on nitrogen absorption from uranium mononitride. The dashed line is for extrapolation beyond the limits of the thermodynamic database.

From Figure 8, it is observed that the reaction in Equation (1) is only spontaneous ($\Delta G < 0$) for temperatures below 200 °C, while the reaction is Equation (2) is never spontaneous ($\Delta G > 0$). Because the composite was initially mixed and pressed as yttrium dihydride and uranium mononitride, it is hypothesized that the yttrium absorbed nitrogen during cool-down after the attempted liquid phase sintering step. With uranium mononitride acting as the excess reagent, the final volume fractions of yttrium nitride, uranium metal, and uranium mononitride were calculated. These values are summarized in Table 4. Table 5 gives the final percent theoretical density of each pellet given the new theoretical densities in Table 4.

Table 4: Calculated compositions of each UN-Y composite batch following conversion of Y to YN during cooldown.

Volume percent Y	Theoretical volume percent YN	Theoretical volume percent UN	Theoretical volume percent U	Composite theoretical density (g/cm^3)
19.25	19.01	68.10	12.89	13.30
20.04	19.85	66.69	13.46	13.25
30.43	31.30	47.48	21.22	12.63
39.15	41.62	30.16	28.22	12.07

Table 5: Percent theoretical density of pellets recalculated for reactions to form YN and U metal.

Pellet ID	Volume percent Y	Final density (g/cm^3)	Percent theoretical density
35-P-19-043	19.25	8.31	62.47
35-P-19-044	19.25	8.42	63.53
35-P-19-056	20.04	8.11	61.20
35-P-19-057	20.04	8.98	67.77
35-P-19-058	30.43	7.37	58.37
35-P-19-059	39.15	7.04	58.28
35-P-19-060	39.15	7.03	58.24

Table 4 shows that the transformation of yttrium to yttrium nitride does not have a significant effect on the volume fraction of yttrium-containing species, but does result in a significant volume fraction of uranium metal. Because yttrium nitride and uranium metal have higher densities than yttrium metal and uranium mononitride, respectively, the theoretical density of the composite material is much higher than the values calculated in Table 2. Thus, the transformed pellets had lower true percent theoretical density than did the as-pressed pellets.

From the XRD results, it was of interest to determine whether phase separation between the three phases was observable and why the pellets exhibited durability during drop tests. To that end, one pellet was mounted in epoxy, lightly polished, and examined in an SEM. An optical image of the polished sample surface is shown in Figure 9, while electron micrographs of the sample interior and edge are given in Figures 10 and 11, respectively.

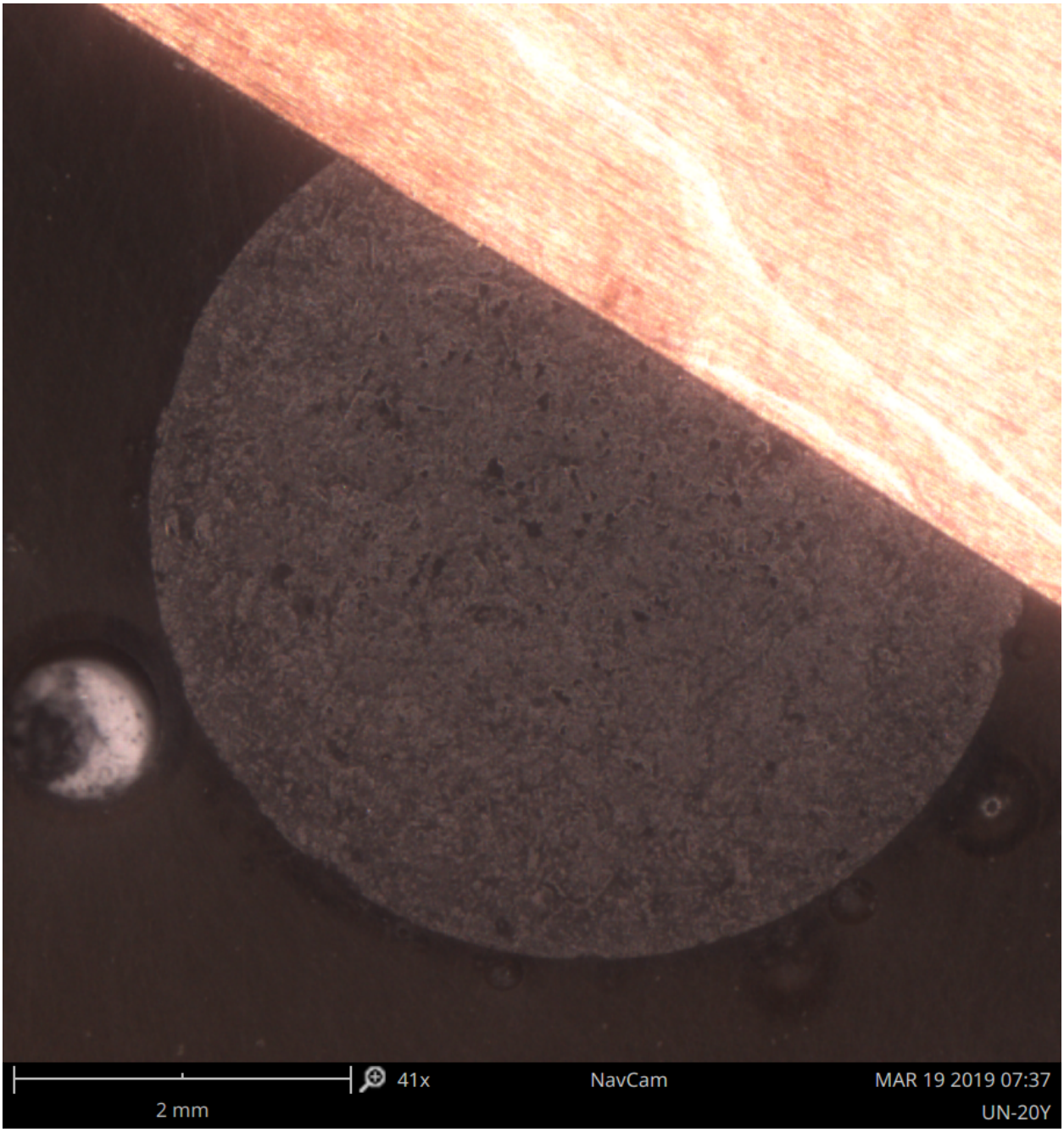

Figure 9: Optical microscopy image of the surface of a UN-20Y pellet.

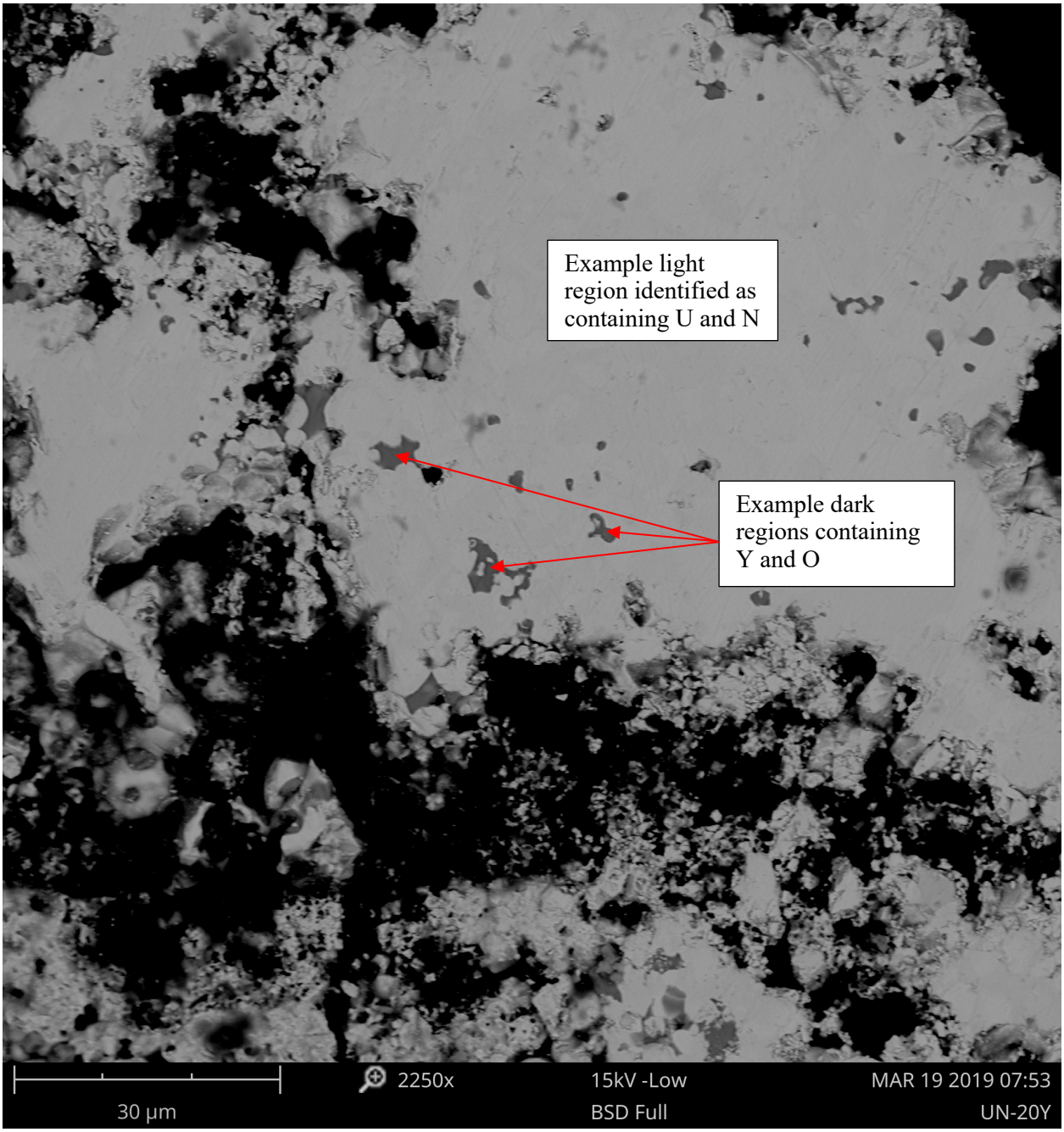

Figure 10: SEM micrograph of a region near the center of a UN-20Y pellet. Light regions were examined using EDS and were observed to contain U, N, and Y. Conversely, dark regions were observed to contain Y and O. Examples of these regions are pointed out in the figure.

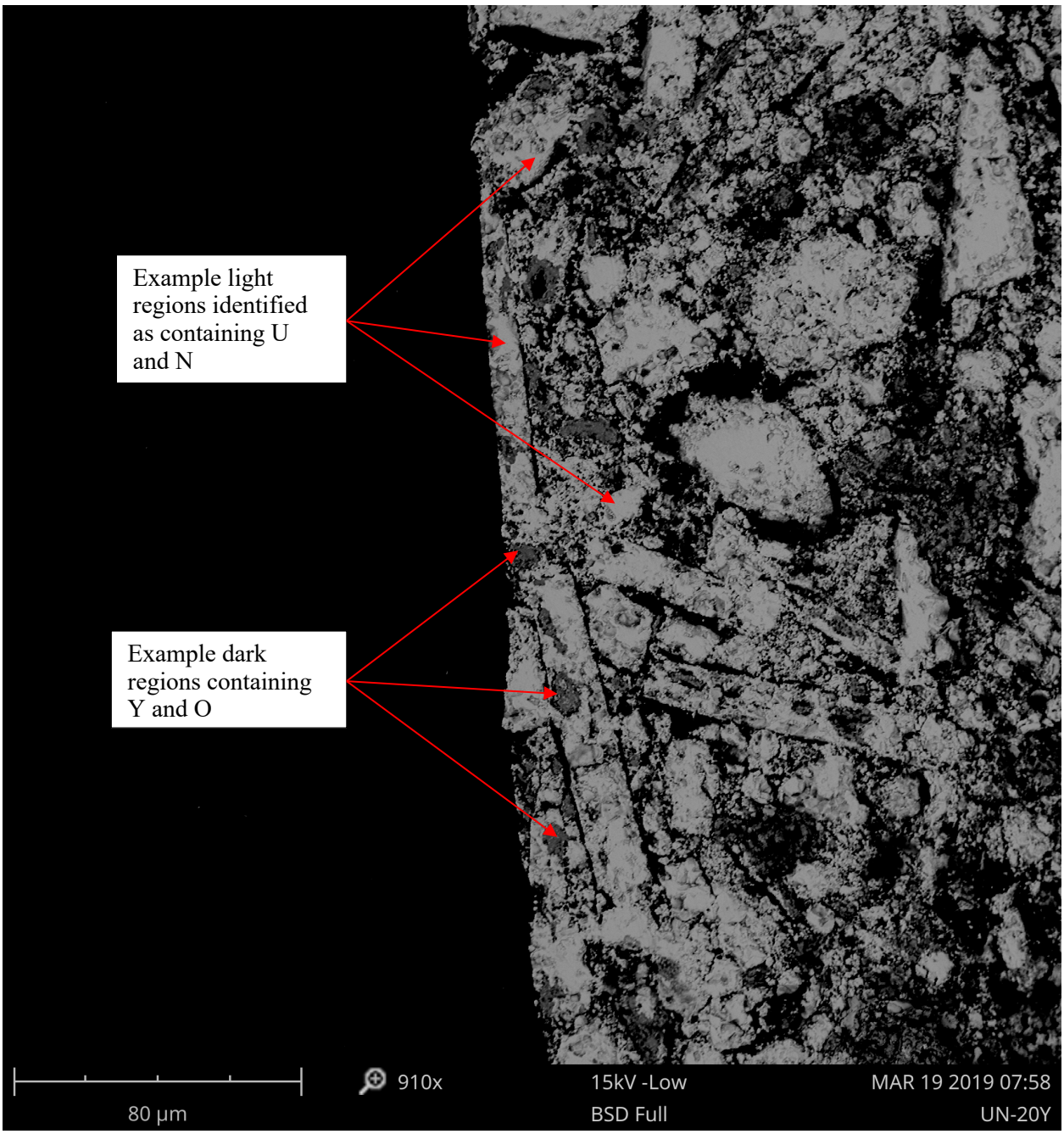

Figure 11: SEM micrograph of a region near the outer surface of a UN-20Y pellet. Light regions were examined using EDS and were observed to contain U, N, and Y. Conversely, dark regions were observed to contain Y and O. Examples of these regions are pointed out in the figure.

Figures 10 and 11 show no significant features, other than exhibiting some densification at the sample surface while still remaining low-density further into the center of the pellet. There does appear to be some anisotropic growth. This could be due to either the yttrium metal or the uranium metal, due to their anisotropic crystal structures (hcp and orthorhombic, respectively) though it is not clear right now. It is likely not due to the uranium mononitride, which has a fluorite structure.

EDS was performed at targeted points to determine if Z-contrast in the SEM might be associated with phase segregation. Lighter regions were determined to be predominantly uranium mononitride, while

darker regions (distinct from porosity) were found to contain significant amounts of yttrium and oxygen. No distinct regions containing uranium metal or yttrium nitride were found. From this result, it is hypothesized that the yttrium nitride and uranium metal oxidized upon removal from the inert glovebox and during polishing.

4. Additional concepts being evaluated

From the result of this L3 milestone, liquid phase sintering as a possible mechanism for developing microstructurally controlled uranium mononitride will need to be re-evaluated. Particularly with regards to metals that have a propensity to nitride. To that end, Ellingham diagrams for nitride formation were developed using ThermoCalc and the SGTE Substances Database 6.0. The results of these calculations are shown in Figure 12.

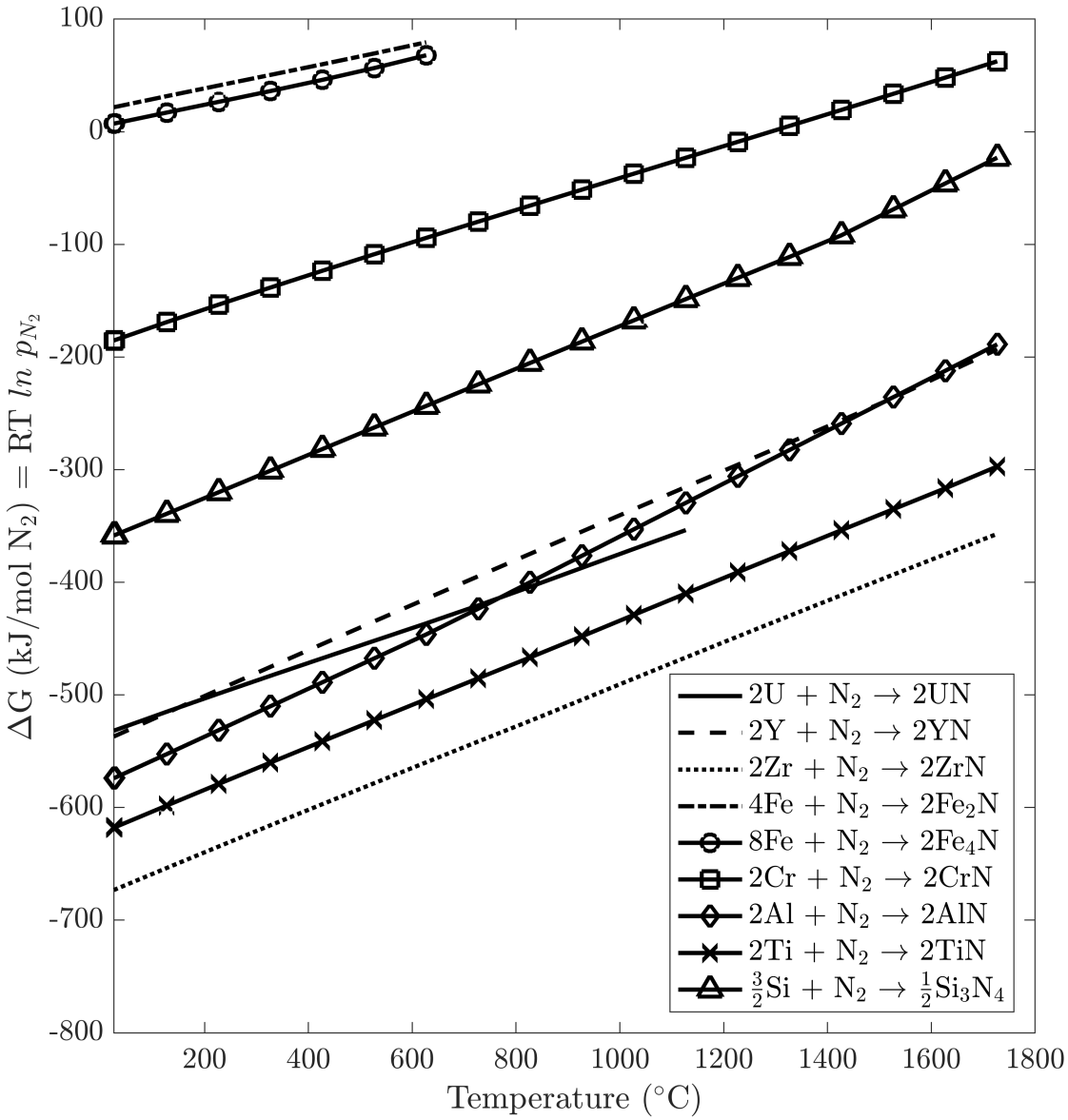

Figure 12: Ellingham diagram for nitriding of various candidate materials for developing microstructurally-engineered uranium mononitride.

Figure 12 plots the Gibbs free energy for nitriding as a function of temperature. This plot also includes nitriding of liquid metal in the calculations, where applicable (i.e. silicon nitride and aluminum

nitride formation). In this plot, the more negative a curve, the more spontaneous the reaction and the more stable the reaction product. The following discussion will relate thermodynamic stability of nitrides with respect to uranium mononitride formation (solid line with no markers). Figure 12 shows potential difficulties for developing microstructurally-engineered uranium mononitride. For example, from this plot, it is observed that zirconium nitride is more thermodynamically stable than is uranium mononitride at all temperatures considered. Because of this, liquid phase sintering uranium mononitride with zirconium metal is probably not feasible, as the zirconium will absorb nitrogen when possible. However, co-sintering of zirconium nitride with uranium mononitride may be a feasible path forward, as zirconium will remain nitride at all temperature regimes and will not lose nitrogen to uranium.

A simple way to interpret Figure 12 is that the elements corresponding to the curves above the uranium mononitride formation curve (less spontaneous nitriding reaction) are good candidates for liquid phase sintering and coating, as they will not absorb nitrogen from the uranium. Conversely, the elements corresponding to curves below the uranium mononitride formation curve (more spontaneous nitriding reaction) may be good candidates for co-sintering, as uranium will not likely remove nitrogen from these compounds. Based on these results and the proven oxidation resistance of some nitrides, such as aluminum nitride and titanium nitride [4], the next steps to addressing the waterproofing of uranium mononitride will include co-sintering with these oxidation-resistant nitrides. Other concepts include co-sintering with oxides that are impervious to oxygen transport, such as alumina, and coating pellets with corrosion-resistant metals (that do not nitride) or ceramics, as noted above.

5. Summary and future work

In an effort to develop microstructurally-engineered uranium mononitride for the purpose of waterproofing, several different approaches were considered, including liquid-phase sintering with oxidation-resistant metals, co-sintering with oxidation-resistant ceramics, and coating. This L3 milestone focused on liquid-phase sintering with yttrium metal, while simultaneously examining the steam-oxidation resistance of several candidate composite components for microstructurally-engineered uranium mononitride. Results indicated that yttrium might be a promising candidate metal for liquid phase sintering due to its resistance to oxidation in steam as compared with zirconium, which is traditionally used in-reactor. Yttrium dihydride powder (for ease of milling) was mixed with uranium mononitride powder in specific compositions, pressed, and heated to above the melting temperature of yttrium so that the yttrium dihydride would dehydride and subsequently melt. However, attempts to liquid phase sintering uranium mononitride with yttrium metal resulted in reaction between the two components to form yttrium nitride and uranium metal, as observed from XRD. The observation of low-density pellets and the formation of uranium metal suggests that liquid phase sintering with yttrium and zirconium (see Future Work) is not a viable path forward at this moment. Thermodynamic calculations showed that this was not possible except at temperatures below 200 °C, indicating that the yttrium nitride formation occurred during cooldown from the attempted sintering step. SEM analysis of the surface of a UN-20Y pellet did not indicate any distinct phase separation of the three phases, though dark regions in the micrographs were found to correspond to high concentrations of yttrium and oxygen. It is hypothesized that the yttrium nitride-rich regions may have oxidized after removal from the inert, argon glovebox for polishing.

The L2 milestone report on waterproofing studies of uranium mononitride (M2FT-19LA020201021) will holistically examine steam oxidation resistance and resistance to reaction with uranium mononitride, as within the scope outlined above. As waterproofing concepts and candidates are identified and evaluated, the matrix of samples to test in steam using TGA will continue to expand. The L2 milestone will focus on all three approaches outlined above: liquid-phase sintering, co-sintering, and coating.

6. Bibliography

[1] N. R. Wozniak and J. T. White, “Determination of the feasibility to waterproof UN for LWR use.” 27-Jul-2018.
[2] B. A. Pint, K. A. Terrani, A. Nelson, S. Parker, and A. Parkison, “High Temperature Steam Oxidation Testing of Candidate Accident Tolerant Fuel Cladding Materials,” Oak Ridge National Lab. (ORNL), Oak Ridge, TN (United States), ORNL/TM-2013/540, Dec. 2013.
[3] S. S. Parker, J. White, P. Hosemann, and A. Nelson, “Oxidation Kinetics of Ferritic Alloys in High-Temperature Steam Environments,” *JOM*, vol. 70, no. 2, pp. 186–191, Feb. 2018.
[4] E. Alat, A. T. Motta, R. J. Comstock, J. M. Partezana, and D. E. Wolfe, “Multilayer (TiN, TiAlN) ceramic coatings for nuclear fuel cladding,” *J. Nucl. Mater.*, vol. 478, pp. 236–244, Sep. 2016.